Modelling of light scattering by gold nanoparticles at optical fibre interfaces

Wang, Xiang; Benedictus, Rinze; Groves, Roger M.

DOI
10.1088/2040-8986/abda87

Publication date
2021

Document Version
Final published version

Published in
Journal of Optics (United Kingdom)

Journal of Optics

PAPER • OPEN ACCESS

Modelling of light scattering by gold nanoparticles at optical fibre interfaces

OPEN ACCESS
IOP Publishing
Journal of Optics
J. Opt. **23** (2021) 035602 (12pp)
https://doi.org/10.1088/2040-8986/abda87

Modelling of light scattering by gold nanoparticles at optical fibre interfaces

Xiang Wang, Rinze Benedictus and Roger M Groves

Faculty of Aerospace Engineering, Delft University of Technology, 2629 HS Delft, The Netherlands

E-mail: Xiang.Wang@tudelft.nl, R.Benedictus@tudelft.nl and R.M.Groves@tudelft.nl

Received 4 October 2020, revised 31 December 2020
Accepted for publication 11 January 2021
Published 18 February 2021

Abstract

Optical fibre backscatter reflectometry is an important technique for Structural Health Monitoring (SHM). In recent years, increasing the intensity of backscattered light in backscatter reflectometry has shown the advantage of improving the signal detection in shape sensing and temperature detection due to the increase of signal to noise ratio and this approach could potentially be used to improve the performance of an SHM system. Doping nanoparticles (NPs) is a method to increase the intensity of backscattered light in distributed fibre optic sensing. The increased intensity of light backscattered by the NPs needs to be investigated to design suitable optical sensing fibres with NPs for backscatter reflectometry. In this work NPs were added to refractive index matching liquid and tested with commercial NP suspensions experimentally between the tips of two optical fibres. An estimate of the intensity of backscattered light from the NPs in this structure was performed by simulation to give a better understanding of the expected levels of intensities of scattered light from NPs in this distributed fibre optic sensing configuration. We present analytical models based on Mie theory and the Monte Carlo Method. Simulated results are presented, for a broad bandwidth Gaussian spectra shape incident light with a central wavelength around 1550 nm, to match the experimental conditions in this work. The novelty is in developing this model for scattered light by NPs at optical fibre interfaces and the evaluation of the possibility of detection by the calculated scattered intensity levels.

Keywords: light scattering model, optical fibre, gold nanoparticle suspension, backscattering

(Some figures may appear in colour only in the online journal)

1. Introduction

Backscatter reflectometry based on optical frequency domain reflectometry (OFDR) for strain or temperature sensing emerged two decades ago [1] and has developed into a technique with millimetres spatial resolution [2–4]. Due to its distributed sensing capability for strain, it has been widely used for Structural Health Monitoring (SHM) in aerospace [5–7] and civil engineering [8].

Backscatter reflectometry uses the backscattered signals along the optical fibre which are caused by the intrinsic refractive index fluctuations along the optical fibre [9]. When the strain changes, the distribution of the scattered light along the optical fibre will be redistributed. By comparing the difference of the original spectra and the spectra after this scattered light has been redistributed, the value of the strain change can be obtained. The strain detection ability makes this technique useful for SHM. It has been used for strain monitoring [5] of an aerospace structure and for the damage detection based on strain [7], etc. Because backscatter reflectometry relies on the backscattered light by the optical fibre and the intrinsic backscattering in optical fibre is small (-100 dB mm^{-1}[10]), one of the limitations of this technique is the low intrinsic backscattering level [11]. By increasing the backscattered signals, the signal to noise ratio will increase, then the sensitivity of measurement will increase.

In order to increase the signal to noise ratio in backscatter reflectometry, several methods have been proposed in recent years used to increase the sensing performance of backscatter reflectometry. One approach is to introduce damage into the core of the optical fibre with a laser. Loranger *et al* [11] proposed a simple way to increase the intensity of scattered light (by about 20 dB) in an optical fibre with ultraviolet(UV) exposure (213 nm, 5th harmonic of a 1064 nm Nd:YAG Laser). The strain resolution and measurement quality improved after UV exposure. A high NA photosensitive fiber under UV exposure showed a low noise level (5 mK or 40 nε). Parent *et al* [12] also used this method and realized a 47 % accuracy improvement in shape sensing in surgical needles. Yan *et al* [13] used an ultrafast infrared(IR) laser (800 nm, Ti:Sapphire Laser) to make nanogratings to increase the intensity of scattered light in an optical fibre (by about 40–45 dB). The defects (nanogratings) are stable and can be used at a temperature of up to 800 °C. Lu *et al* [14] improved the accuracy of temperature detection by fabricating random fibre gratings in an optical fibre with a femtosecond IR laser (800 nm).

Doping nanoparticles (NPs) into the core of an optical fibre is another very important approach to increase the backscattered light and generally the backscattered light enhancement is higher than the method of introducing damage with a laser. For strain sensing, Blanc and Dussardier [15] described different methods of making NPs in silica optical fibre and analysed the obtained losses with Rayleigh scattering. Molardi *et al* [16] investigated the characteristics of magnesium oxide (MgO) doped optical fibre and obtained a 50 dB scattered light increase experimentally. They pointed out that this doped fibre could be used for spatial multiplexing in optical backscatter reflectometry. Beisenova *et al* [17] presented the experimental results of three dimensional (3D) shape sensing with an MgO doped optical fibre in a spatial multiplexing structure for an epidural needle. These results showed the sensing improvement caused by doping NPs. As mentioned above, strain sensing is also important for SHM. Therefore, the phenomenon of light scattered by NPs in optical fibre drew our attention. We think that the improvement of signal to noise ratio in strain sensing by NPs may also show potential for Structural Health Monitoring based on strain detection.

Due to the increase in the backscattered light in an optical fibre by doping with NPs and the potential of being used for improving the strain detection for SHM by increasing the signal to noise ratio, the characteristics of the scattered light in the optical fibre need to be investigated. In practice, manufacturing optical fibres with NPs is not easy in an optical laboratory and a careful design is needed. In order to investigate the behaviours of NPs in fibre optic sensors, we proposed a simple setup to investigate the characteristics of NPs for further development in SHM [18]. It is to drop refractive index (RI) matching liquid between two optical fibre tips and to study the scattering characteristics for different NPs under different experimental parameters. By eliminating the influence of the reflections from the optical system, the detected backward signals caused by the scattering from NPs in RI matching liquid can be obtained. Then by constituting the relationship between scattered light signals from NPs and scattered light by NPs in the optical fibre, the goal of evaluating the scattered light by NPs in the optical fibre can be achieved. There has also been research in using NPs to coat the surface of the optical fibre. However, with this approach, the levels of scattered light need to be treated carefully because the intensity of scattered light from low concentration NPs are generally low and could likely be lower than the sensitivity of a conventional optical detection system.

There has also been some research in showing methods to attach gold NPs or thin layers to the optical fibre for use as sensors [19–22]. Although this could be an approach to investigate the behaviour of NPs, the thin gold layers will cause higher reflections than the method of dropping RI matching liquid containing NPs. Compared with attaching NPs on the interfaces of optical fibre, dropping RI matching liquid containing NPs at optical fibre interfaces is closer to the case of NP-doped optical fibre. Another advantage for dropping RI matching liquid containing NPs is that a series of useful light signals scattered by the NPs in the volumes of RI matching liquid can be obtained while only one the surface reflection signal is obtained by attaching gold to an optical fibre end tip. In addition, the shape and size of NPs in liquid can be well-controlled, it is another advantage of this method.

In order to acquire the scattered light intensity levels by the gold NPs at optical fibre interfaces, a model of light scattering by gold NPs at optical fibre interfaces needs to be built to evaluate the intensity of light scattering levels. Simulations of the intensity of scattered light from NPs need to be performed to give a good understanding of these intensity levels of scattered light in the liquid containing gold NPs. The model for backscattered light for three different sizes of NPs in order to determine suitable experimental conditions will be shown in this paper.

This paper is organized in five sections. The first section is the Introduction. The model for the simulation is given in section 2. The intensities of scattered light with the coupling model are simulated from 10 to 400 nm size gold NPs with the Monte Carlo method and experiments with commercial 10, 100 and 400 nm NP concentrations are compared with the calculated results in section 3. This is followed by a discussion in section 4. Section 5 is the conclusions.

2. Experiment setup and model

In this section, the experimental setup used for modelling is introduced first in section 2.1. The model of light propagation at optical fibre end tips is then described in section 2.2. The model of scattered light by NPs and the light recoupled into the upper optical fibre will be described in section 2.3.

2.1. Experimental setup

We used the experimental setup shown below in figure 1 to collect back-scattered light from NPs suspended in liquid between the two optical fibre tips. Figure 1(a) shows a diagram of the experimental setup. It includes a 1550 nm

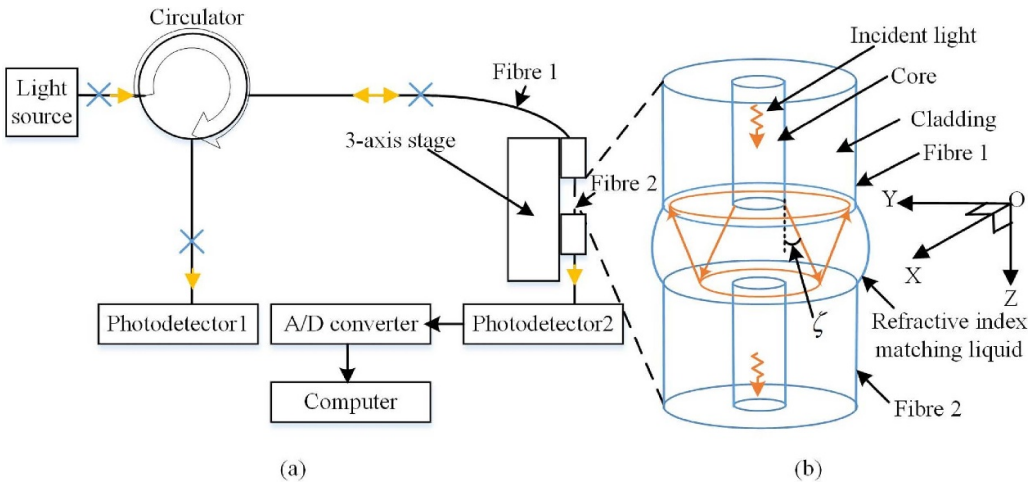

Figure 1. Experimental setup. (a) Diagram of the experimental setup. The yellow arrows represent the directions of light propagation. The blue crosses are the optical fibre connectors. (b) Enlarged figure of the region of the two optical fibre end tips. Optical fibres are shown in blue. Light is in yellow with its propagating directions. ζ is the divergence angle in liquid. A coordinate system is defined with the origin (O) at the centre of the end surface of the upper fibre.

central wavelength superluminescentdiode (FESL-1550-20-BTF, Frankfurt Laser Company), an optical circulator (6015-3-APC Fiber Optic Circulator, Thorlabs), a 3-axis translation stage (MAX373D/M, Thorlabs), two photodetectors (Photodetector 1: PM20C (Thorlabs), Photodetector 2: PDB420C Monitor+, Thorlabs), an analog-to-digital (A/D) converter (PicoScope 6402A, Pico Technology), a computer and a universal serial bus (USB) microscope.

Light emitted from the light source goes via the circulator to the upper optical fibre (Fibre 1: single mode fibre 1550BHP, Thorlabs) on the 3-axis stage. The end tip of Fibre 1 is fixed and Fibre 2 is clamped onto this 3-axis stage. Liquid containing NPs is dropped into the gap between the end tips of the lower optical fibre (Fibre 2: single mode fibre 1550BHP, Thorlabs) by a volumetric dispenser (PreciFluid). For the modelling, refractive index matching liquid (refractive index 1.4520) containing homogeneous gold NPs was dropped between two optical fibre end tips. With the use of refractive index matching liquid, the influence from the reflection from the optical fibre end tips are reduced in order to focus on the signal scattered by NPs. For the experiment, a commercial gold NPs suspension in citrate buffer (Sigma-Aldrich) is used. The end tips shown in figure 1(b) are cleaved at 90% in the model (Note: angle polished connectors are used as end tips in the experiment to further reduce the reflection from optical fibre end tips). Figure 1(b) shows more details of this fibre end tips gap for modelling. Some of light is coupled into the lower optical fibre through the RI matching liquid containing gold NPs and detected by photodetector 2. Optical fibres are shown in blue in figure 1(b). Light collected by photodetector 2 can be used for detecting the extinction from the gold NPs, but in this paper we only analysed the backscattered light from the NPs. Some of the light scattered or reflected back to the upper optical fibre and the light is collected by photodetector 1 via the circulator. If the refractive index of the refractive matching liquid matches the refractive index (RI) of the optical fibres, the reflected light from the end tips of the gap will be eliminated and the percentage of scattered light from the NPs to the total obtained light at photodetector 1 will improve. Note: even though refractive index liquid is used, there remain reflections from the surfaces of the optical fibre end tips and the collected light by photodetector1 is a combination of both the light scattered by NPs and the reflection of the end tips.

2.2. *Light propagation between two optical fibre end tips*

In order to model the experimental setup more accurately, the spectrum of the light source is modelled with a Gaussian spectrum. There is a good similarity of the spectrum from the superluminescent diode (FESL-1550-20-BTF, Frankfurt Laser Company) and the Gaussian spectrum ($R^2 = 0.97$). Therefore, the spectrum of the incident light is modelled as Gaussian spectra shape light according to the shape of the superluminescent diode and the total power is normalized to I_0 as:

$$I(\lambda) = I_0 \times \left(\frac{2\sqrt{\ln 2}}{\Delta\lambda_{\mathrm{FWHM}}\sqrt{\pi}} \times \exp\left(-4\ln 2 \left(\frac{\lambda - \lambda_c}{\Delta\lambda_{\mathrm{FWHM}}} \right)^2 \right) \right), \tag{1}$$

where I_0 is the power of the incident light. λ is the wavelength of the light; $\Delta\lambda_{\mathrm{FWHM}}$ is the full width at half maximum (FWHM) of the spectra. λ_c is the central wavelength. λ, $\Delta\lambda_{\mathrm{FWHM}}$ and λ_c are in nm.

For the light power density distribution at the end of the upper optical fibre we use a Gaussian distribution for this single mode optical fibre and the power density distribution can be expressed as

$$I_{\text{in optical fibre}}(r, \lambda) = \frac{I(\lambda)}{(2\sigma_0)^2\pi/2} \times \exp\left(-2 \left(\frac{r}{2\sigma_0} \right)^2 \right), \tag{2}$$

where r is the radial distance to the centre of the cylindrical optical fibre and $r = \sqrt{x^2 + y^2}$. (x, y) is the position. $2\sigma_0$ represents the mode field radius of the incident light in the upper of optical fibre.

In the liquid, the transmitted light will disperse in RI matching liquid. The divergence angle ζ for a single mode fibre is small and can be calculated from its numerical aperture (NA) and the RI of RI matching liquid. The side reflection caused by the external boundary of the RI liquid is negligible. The shape of the light propagating in the liquid can be estimated by the geometric divergence:

$$I_{\text{wavelength}}(x,y,z,\lambda) = T_1 \times \exp(-\alpha z) \times I(\lambda) \times \frac{1}{(2\sigma_0/k(z))^2 \pi/2} \times \exp\left(-2\left(\frac{r}{2\sigma_0/k(z)}\right)^2\right) \quad (3)$$

$$k(z) = \frac{r_{\text{core}}/\tan\zeta}{z + r_{\text{core}}/\tan\zeta}, \quad (4)$$

where T_1 is the transmittance between the optical fibre to liquid surface and can be calculated using the Fresnel equation, α is the light loss coefficient in the liquid and can be expressed by the sum of the loss by absorption by the liquid and the extinction by NPs in the liquid; and $k(z)$ is the distribution amplification ratio at this position. The propagating wave is estimated as a plane wave in equation (3) because of the small divergence angle (about 5°), so the distribution amplification ratio is only related to the Z direction. Using the RI at a central wavelength of 1550 nm for the calculation, the divergence angle ζ can be regarded as a constant for different wavelengths for the calculation. ζ can be deduced by the relation $NA = n_{\text{liquid}} \sin\zeta$.

The light propagating between the two optical fibre end tips will be reflected by the two end surface, but the reflected light is negligible as analysed below. As shown in figure 1(b), part of the light will be reflected at the surface of the lower optical fibre and will then propagate until reaching the surface of the upper optical fibre. The reflected light can also be expressed by equation (3) because the lower optical fibre has the same geometry as the upper optical fibre.

The reflected light can be expressed as

$$I_{\text{wavelength,backward}}(r,z',\lambda) = \frac{T_1 R_2 I(\lambda)}{(2\sigma_0/k(z'))^2 \pi/2} \times \exp\left(-2\left(\frac{r}{2\sigma_0/k(z')}\right)^2 - \alpha z'\right), \quad (5)$$

where R_2 is the reflectance at the lower optical fibre interface and can be calculated according to the Fresnel equation; α is the attenuation caused by the absorption of liquid and extinction from NPs; $z' = 2\,h - z$.

Reflected light will propagate until the interface of the upper fibre. Considering that only light incident on the core of optical fibre can be re-coupled, the intensity of reflected light coupled into the upper optical fibre can be expressed as the integral:

$$I_{\text{reflect}} = \int_{S_{\text{core}}} \int_{\lambda} T_1 I_{\text{wavelength,backward}}(x,y,2\,h,\lambda)\,\mathrm{d}\lambda\,\mathrm{d}S_{\text{core}}, \quad (6)$$

where S_{core} is the region of the core of optical fibre.

The back-propagating light will also be reflected at the surface of the upper optical fibre. It is not shown in figure 1(b) and has not been taken into consideration in the analyses. The reason for this is that when RI matching liquid is used the reflectance is very low at the interfaces (e.g. only about 4.750×10^{-7} with the RI of optical fibre of 1.450 and the RI of the liquid at 1.452) and when the light reflects twice the intensity of the light will be lower than the square of this reflectance. Light reflected multiple times also is neglected. Now we know that transmitted light is the main factor affecting scattering by NPs as compared to reflected light. In the next part, we will discuss the scattered light by NPs and the scattered light re-coupling into the upper optical fibre.

2.3. Scattered light coupling model

The concentrations of the NPs in the liquid are low and meet the requirements for single scattering [23] (optical depth $\tau = cC_{\text{ext}}z < 1$) in this model. c is the concentration of the NPs, C_{ext} is the extinction cross-section and z is the path depth. In this case, only light scattered once by the NPs is taken into account. The intensity of scattered light by single particles can be added because of the random positions of the NPs in liquid and the movement of the NPs cause the decoherence. The concentration of NPs in a unit volumetric liquid is assumed to be a constant. Due to the low concentration of the NPs, it is assumed that the wavefront will not be disturbed by the NPs but will attenuate from the absorption of the medium and the extinction by NPs. Figure 2 shows the modelled configuration with NPs. The blue dots in figure 2 represent NPs in random positions in the RI liquid volume. The sizes of the NPs are assumed to be the same and they are assumed to be spheres.

Considering the size of the NPs, the incident light can be considered as a plane wave incident on each NP. Therefore the scattered light by each NP can be calculated by Mie theory [24]. The smaller NPs are more in Rayleigh scattering range and the larger NPs are in the Mie scattering range. It was decided to adopt Mie theory for the calculations as this approximates to the Rayleigh scattering calculation at smaller wavelengths. According to Mie theory, the intensity of light scattered by a spherical particle verses angle θ' can be expressed as

$$I_s(\theta',\varphi',r',\lambda) = \frac{(\lambda/n_{\text{liquid}})^2}{4\pi^2 r'^2}\left(\frac{i_1(\theta') + i_2(\theta')}{2}\right). \quad (7)$$

It is described in a spherical coordinate system as shown in the enlarged picture of figure 2. The origins are set at the centres of NPs (O_i). θ' is the scattering angle, r' is the distance between the center of the spherical gold NP to the detection

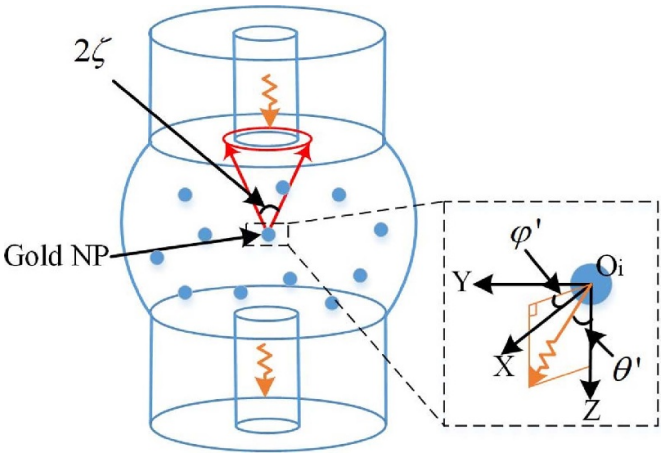

Figure 2. Model of re-coupled scattered light from NPs (a) The enlarged picture of the region of the upper optical fibre surface shows the overlap area by the edge of scattered light on the upper fibre end tip (red) the core of optical fibre (blue); (b) the enlarged picture of a NP with its spherical coordinates whose Origin is at the centre of this NP.

point, $i_1(\theta')$ and $i_2(\theta')$ are called the scattering intensity functions, the unit of λ is μm and the unit of r' is μm. The parameters $i_1(\theta')$ and $i_2(\theta')$ can be obtained by Mie theory [24].

The scattered wave is regarded as a spherical wave whose centre is at the centre of the NP. The intersection of the scattered light with the acceptance angle of the optical fibre is shown by a red cone in figure 2. The base of the red cone on the end surface of the upper optical fibre is a red circle as shown in figure 2. The blue circle in figure 2 is the core of optical fibre. There is an overlap area between the two circles. The overlap area is regarded as the area in which the light can be re-coupled into optical fibre. When integrating the light propagating into this overlap area, the intensity of re-coupled light scattered by one NP can be obtained.

However, the integral of all the light within the angles in the overlap area is complicated when the NPs are not at the centre of the propagating light. To simplify the calculation, we use the mean value of the intensity density of the scattered light in the backward direction (π) and in the edge of the red cone ($\pi-\zeta$) as the mean-value for intensity density in this overlap area. The mean-value for intensity in this overlap area can be expressed as

$$I_{\text{mean}} \approx \frac{I_s(\pi,\varphi',r',\lambda)+I_s(\pi-\zeta,\varphi',r',\lambda)}{2}. \tag{8}$$

Therefore, the intensity of the scattered light in the cone is estimated as I_{mean}. The mean value for intensity density in this overlap area times the area of spherical cap is regarded as the intensity of the scattered light within the cone.

Considering the divergence angle is small, the area of the cross-section of the spherical cap on the surface of the upper optical fibre is estimated to be the area of the spherical cap. Therefore, the intensity of scattered light within the cone can be estimated by the mean-value of the intensity density in this overlap area times the area of the projection of the spherical cap on the surface of the upper optical fibre.

Because we use the mean value of scattering, the calculation speed can be accelerated by considering the ratio of the scattered light incidents on the core of the upper optical fibre end tip. We define the overlap ratio as the percentage of the overlap area of the core of optical fibre to the area of the spheres whose centres are at the centre of the NPs cut by the end tip of the optical fibre. It is the coupling efficiency of light scattered by NPs coupled to upper side optical fibre end tip in this paper. The overlap ratio γ can be expressed as

$$\gamma = S_{\text{overlap}}/S_{\text{cone}}, \tag{9}$$

where S_{overlap} is the area of the overlap area; and S_{cone} is the area of the cross-section of the spherical cap on the surface of the upper optical fibre.

Therefore, the intensity of re-coupled scattered light by one NP at the wavelength λ can be estimated by:

$$\begin{aligned} I'_s(\lambda) &= \gamma \int_{\pi-\zeta}^{\pi} \mathrm{d}\theta' \int_0^{2\pi} I_{\text{mean}} r'^2 \sin\theta' \,\mathrm{d}\varphi' \\ &= \frac{(\lambda/n_{\text{liquid}})^2(1-\cos\zeta)\gamma}{4\pi} \\ &\quad \times \left(\frac{i_1(\pi)+i_2(\pi)}{2} + \frac{i_1(\pi-\zeta)+i_2(\pi-\zeta)}{2}\right). \end{aligned} \tag{10}$$

Then, the total scattered light that meets this requirement and can be recoupled into the upper optical fibre can be expressed as

$$\begin{aligned} I_{\text{recouple}} = \int_V cT_1 \Bigg(\int_\lambda & I_{\text{wavelength}}(x,y,z,\lambda) I'_s(\lambda) \\ & \times \exp(-\alpha z)\,\mathrm{d}\lambda \Bigg) \mathrm{d}V, \end{aligned} \tag{11}$$

where V is the integral volume, c is the concentration of NPs. Equation (11) mainly includes the light transmission(T_1 and $I_{\text{wavelength}}$), the scattering by the NPs and recoupling into optical fibre (c, I'_s) as well as the light attenuation ($\exp(-\alpha z)$) when the light propagates back.

3. Simulated and experimental results

3.1. Simulations with the Monte Carlo method

We used the Monte Carlo Method [25, 26] with N iterations to estimate the scattered intensity from NPs. N(1000) points (x, y, z, λ) were chosen for each spatial resolution for 6 times. (x, y, z) were randomly distributed in the integral cuboids and the wavelength (λ) was randomly chosen from the range $\lambda_{\min} = 1480\,\text{nm}$ to $\lambda_{\max} = 1620\,\text{nm}$. (In this wavelength range the power of the light accounts for about 99.4% of I_0).

According to the Monte Carlo Method, the approximation of equation (11) can be expressed as

$$\begin{aligned} I_{\text{recouple}} = \sum_{n=1}^{N} \frac{1}{N} & cT_1 I_{\text{wavelength}}(x,y,z,\lambda) \\ & I'_s(\lambda) \frac{1}{1/V_c(\lambda_{\max}-\lambda_{\min})}. \end{aligned} \tag{12}$$

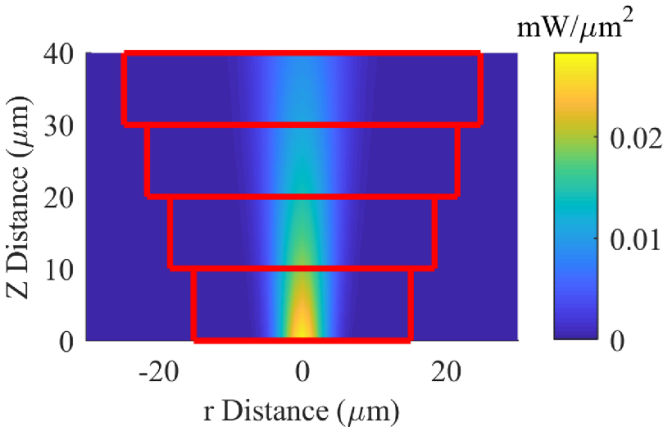

Figure 3. The integrated regions along the propagating of light (The red rectangles represent the integral cuboids with axial resolution 10 μm, length and width of $3\sigma(z)$ at the centre of each spatial intervals (z_{mean})).

We chose 10 μm as the axial resolution Δz in order to show the re-coupled scattered light distribution in the Z direction. The distance between the two optical fibre tips was set to 1 mm. In each axial resolution region we integrated all of the scattered light which can be re-coupled into the optical fibre, so that the integral Z distance is 10 μm. In the X and Y directions we restricted the integral range in cuboids, whose height is the axial resolution, length and width are $3\sigma(z)$ at the centre of each spatial intervals (z_{mean}). Only the NPs in these cuboids $V_c (V_c = (3\sigma(z_{\text{mean}}))^2 \Delta z)$ were taken into account as shown in figure 3.

The diameters of spherical gold NPs are chosen to be from 10 to 400 nm. The step in size change is set at 30 nm and the concentrations are set at 1×10^8 ml^{-1} so that the concentrations are low for all different size of gold NPs. For the 400 nm size gold NPs, the volume ratio is only about 3.35×10^{-6}.

We use the refractive index of gold from Johnson and Christy [27]. The original data of RI of gold is shown with error bars in figure 4.

The RI of gold is a function of the incident light wavelength. Based on the data trends, a third order polynomial fitting curve was used for the real part of the gold RI while for the imaginary part of the gold RI a linear fitting curve was used. The fitting was made by the software Origin 2019 (OriginLab Corporation) and the fitting region is from 1088 nm to 1937 nm. The obtained expressions for the real and imaginary parts of the gold RI are:

$$n_{Au} = -2.72440 + 0.00607 \times \lambda - 4.18591 \times 10^{-6} \times \lambda^2 + 1.04432 \times 10^{-9} \times \lambda^3, \quad (13)$$

$$k_{Au} = -1.35038 + 0.00781 \times \lambda, \quad (14)$$

where the unit of wavelength of the incident light is nm. Other parameters used for calculations are listed in table 1.

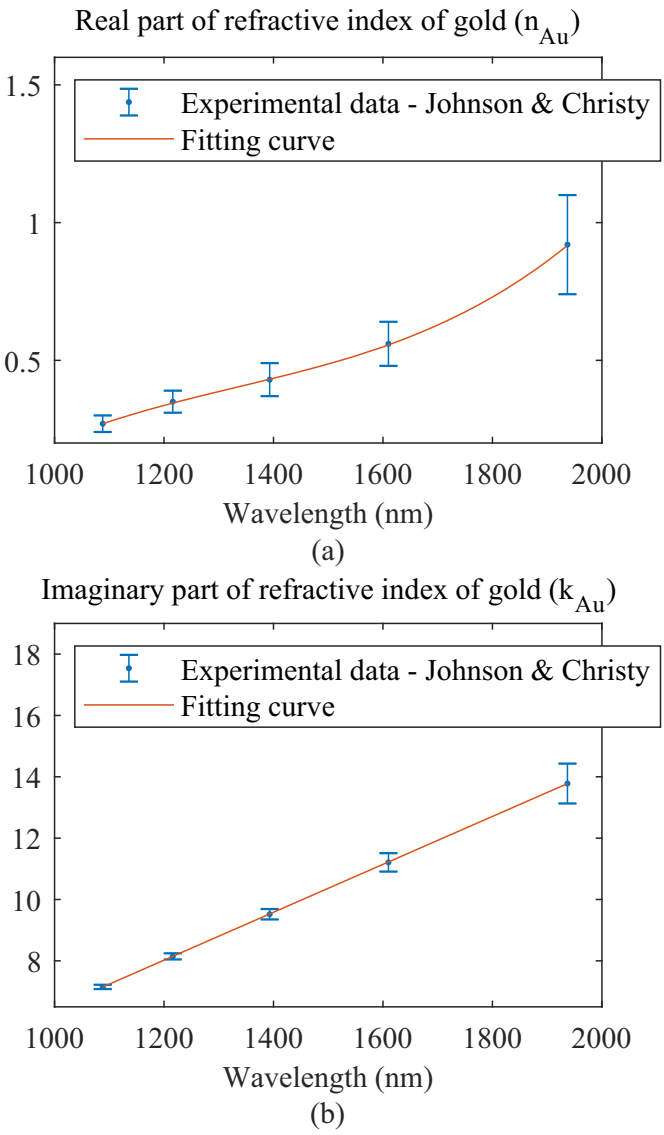

Figure 4. The refractive index of gold (Au) and its fitting plot. (a) The real part (n) of refractive index of gold verse wavelength. (b) The imaginary part (k) of refractive index of gold verses wavelength [27].

Because the concentration is low, the extinction from NPs was neglected. Therefore, $\alpha = 0$ in calculation. The calculation of scattering intensity functions utilize the MatLab code from Matzler's paper [31].

The simulations were processed in Matlab R2019a (The MathWorks). Figure 5 shows the results.

It can be seen from figure 5(a) that the accumulated power increases slowly as the Z distance increases. When the size of NPs increases at the same Z distance the power increases quickly. When the Z distance is above 500 μm and the diameters of NPs are above 250 nm, the accumulated power is above 1 nW. The scattered power decreases dramatically when the size of the NPs is below 50 nm. At a size of about 50 nm, the scattered light is only 0.1 pW. Below a size of about 40 nm, the scattered light is below 0.01 pW. Figure 5(b) is the corresponding error to figure 5(a). The errors are below 10%. Most of the errors are created at the region near the origin of Z direction.

Table 1. The parameters used for the calculation in this work.

Parameter	Symbol	Value for calculation
Central wavelength	λ_c	1550 nm [28]
Light source bandwidth	$\Delta\lambda_{\mathrm{FWHM}}$	60 nm [28]
Incident light power	I_0	1 mW
Core radius of 1550BHP	r_{core}	4.5 μm [29]
RI of 1550BHP	n_{fibre}	1.4511 [29]
NA of 1550BHP	NA	0.13[29]
Mode field radius	$2\sigma_0$	4.75 μm [29]
RI of RI matching liquid	n_{liquid}	1.4520 (near Series A, Cargille [30])
Concentration of gold NPs	c	$1 \times 10^8 \mathrm{ml}^{-1}$

3.2. Case study with experiments

Three different sizes of gold NPs (10, 100 and 400 nm) were evaluated by the Monte Carlo calculation and experimental tests. The parameters of these NPs are listed in table 2.

The axial resolution used in Monte Carlo calculation was set of 12 μm which is similar to the axial resolution of optical coherence tomography (OCT) system [28] and N was set of 10 000 (calculation time is about 1 h with the processor Intel Xeon W-2123 CPU) in each axial resolution region. It was assumed that the gold NPs had been successfully transferred to RI liquid (RI is 1.4520) and the concentrations used were the mean values of the concentrations given in table 2. Figure 6 shows the results with relative dispersion errors. The relative dispersion error is defined as

$$E_{\mathrm{dispersion}} = \left|\frac{s}{\bar{x}}\right| \times 100\%, \tag{15}$$

where s is the sample standard deviation and $\bar{x}$ is the mean value of the samples. Figures 6(a)–(c)'s embedded graphs show the corresponding relative dispersions of figures 6(a)–(c) respectively and it can be seen that the results have low dispersion (below 8%). The error bars in figures 6(a)–(c) also show the relative dispersion errors.

From this calculation, the light reflection from the upper fibre interface can be calculated as 96.1 pW if the incident light is 1 mW (about −70 dB relative to incident light power). Light reflected from the lower optical fibre interface and re-coupled into the upper fibre is 0.104 pW (about −100 dB). It can be seen from figure 6(a) that the scattered light from gold NPs in refractive index liquid decreases along the Z direction from about 0.03 pW. Note this is much smaller than the light reflection from the optical fibre end tip (96.1 pW). This signal is so weak that it would be a challenge to detect it with direct detection with the detection system shown in figure 1. In figure 6(b), it can be seen that the scattered signal increases a lot when the NPs' size increases 10 times from 10 to 100 nm even if the concentration decreases by 156 times (see table 2). The maximum value is also near the upper optical fibre end tip and the signal decreases from about 25 pW, which is also a week signal for direct detection. When the size of the NPs increases 4 times from 100 to 400 nm, even if the concentration decreases about 20 times, the scattered light increases. From figure 6(c), it can be seen that the scattered light decreases along the Z direction from about 1.4 nW. This would be an observable signal within the detection range of the PM20C photodetector and compared with the reflections from the upper optical fibre it is also a relatively high signal.

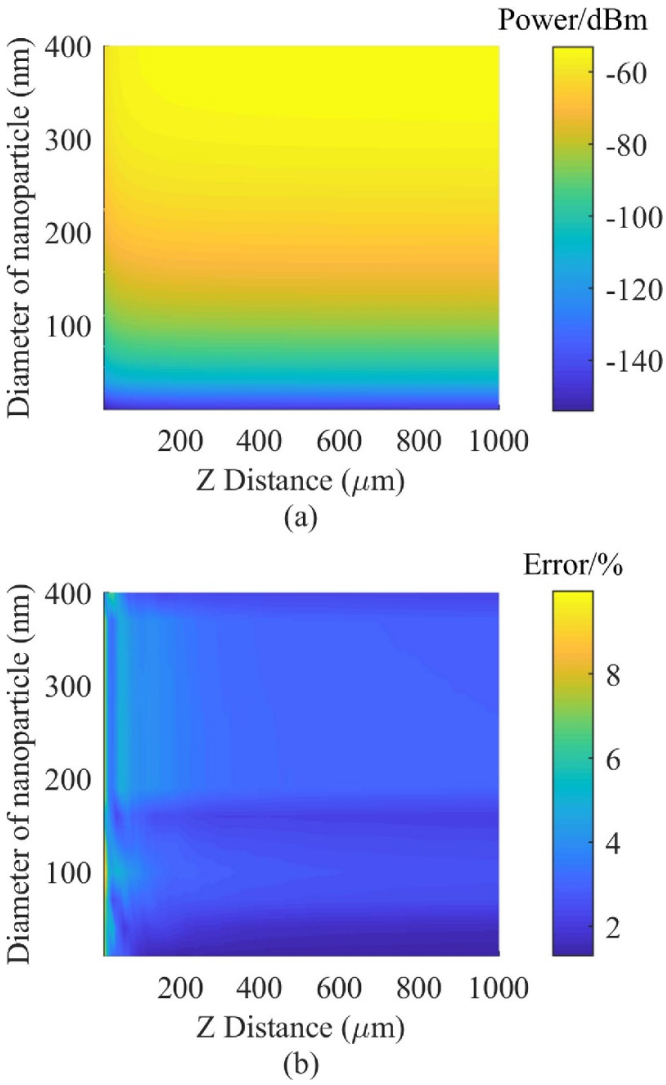

Figure 5. Accumulated scattered light by NPs along the Z direction (The input power is 1 mW and the concentrations of gold NPs are 1×10^8 ml^{-1}). (a) The scattered light power along the Z direction versus different size of NPs (0 dBm = 1 mW); (b) the errors of the results for the calculated accumulated scattered light power.

However, it is not easy to transfer gold NPs to refractive index liquid. In our former work [18], we tried to transfer commercial gold NPs suspension in citrate buffer (Sigma Aldrich) to refractive index liquid (Cargille). The experimental results showed that the transferring process is not efficient enough. Therefore, in this work we dropped the commercial gold NPs suspension directly onto the optical fibre end tips to obtain the scattered light intensity.

Due to the mismatching of refractive indices, there are relatively high reflections from the end tips of optical fibres. If

Table 2. The parameters of experiment samples.

Sample	Concentration [32]	Gold volume ratio
Gold NP 10 nm	5.38×10^{12}–6.58×10^{12} ml^{-1}	3.131×10^{-4}%
Gold NP 100 nm	3.45×10^{9}–4.22×10^{9} ml^{-1}	2.008×10^{-4}%
Gold NP 400 nm	1.60×10^{8}–2.10×10^{8} ml^{-1}	6.199×10^{-4}%

we consider the refractive index of commercial gold NPs suspensions as 1.33, which is the same as the refractive index of water, the calculated reflected light from the upper optical fibre end tip is about 1.9 μW which is much higher than the scattered light by NPs. In order to increase the percentage of the scattered light and to decrease the reflection, we designed a setup to reduce the reflections from end tips with angle polished connectors as shown in figure 7 (the upper optical fibre end tip is connected to the optical circulator; the lower connector has been fixed with epoxy to prevent its position changing). The two connectors are fixed with special designed aluminium clamps on the 3-axis stage. A volumetric dispenser (PreciFluid) was used to dropping liquid to the optical fibre end tips' gap. A USB microscope was used to view the liquids drops.

By rotating the lower connector, a relatively low reflection was obtained. Then, we proceeded to separately drop 400 nm gold NP suspension, 100 nm gold NP suspension, 10 nm gold NP suspension and buffer liquid. The buffer liquid was generated by collecting the liquid supernatant from the 400 nm gold NP suspension by a centrifuge (Centrifuge 5702, Eppendorf) in 5 min and 4300rpm. Before each dropping process, the surfaces of the optical fibre tips were cleaned carefully with disposable wipes (Kimtech) using acetone.

In order to increase the signal obtained at PM20C, we increased the input light at the upper optical fibre end tip to 3.00 mW. The experimental results are shown in figure 8. The orange bars in figure 8(a) show the situations when no liquid was dropped at the optical fibre end tips. The mean value is about 5.99 nW and the standard deviation is about 1.40 nW. The blue bars in figure 8(a) show the results of dropping the 400 nm gold NP suspension into the gap. It shows a large distribution from about 4.38 nW to about 20.89 nW. The mean value of it is about 6.49 nW. The blue bars in figure 8(b) show the results of dropping the buffer liquid into the gap. The mean value of it is about 2.31 nW and the standard deviations is about 0.30 nW. The red bars in figure 8(b) show the results of dropping the 100 nm gold NP suspension into the gap. The mean value of it is about 2.21 nW. The yellow bars in figure 8(b) show the results of dropping the 10 nm gold NP suspension into the gap. The mean value is about 2.19 nW.

Figure 9 shows the calculated results compared with experimental results. The calculated results are based on the data in table 2, the RI of water used was 1.33 and RI of RI matching liquid used is 1.4520. The input power at the upper optical fibre is 3 mW. The axial resolution used in the Monte Carlo calculation was set at 12 μm, N was set at 1000 in each axial resolution region.

Figure 9(a) shows the reflected power for the three different cases in water. In order to show these results in the same

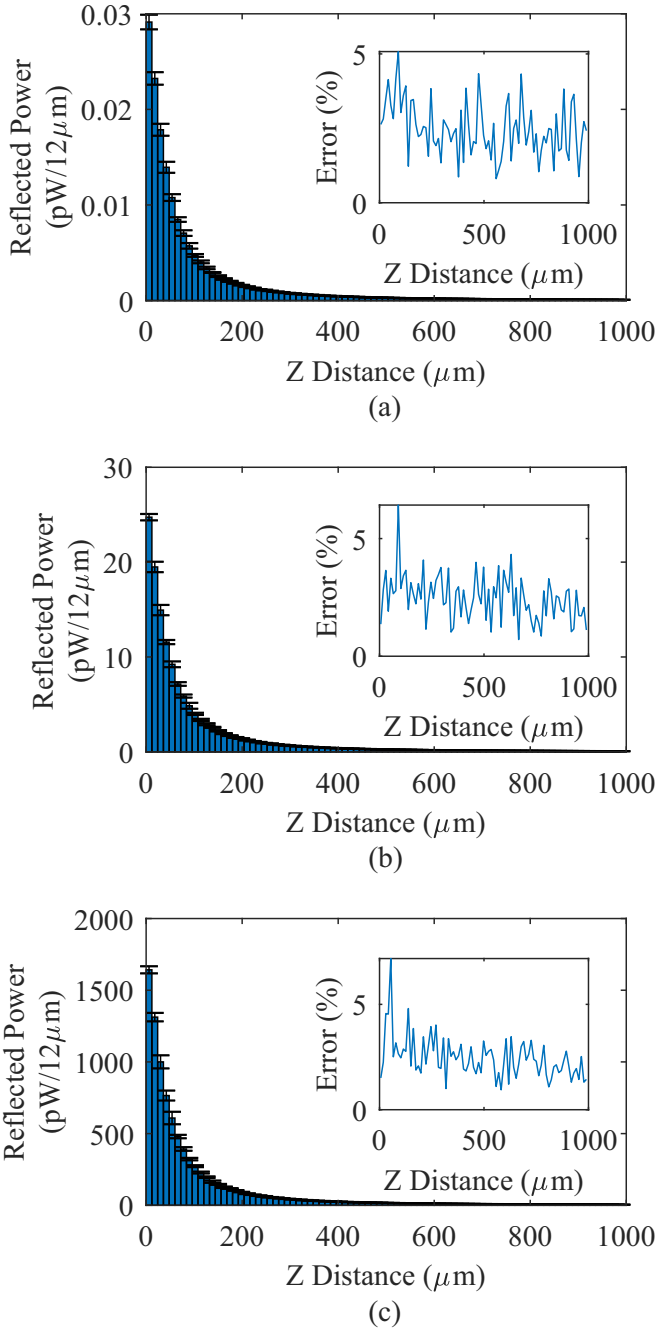

Figure 6. Estimated reflected power values with Monte Carlo Method with axial resolution 12 μm. (a) 10 nm diameter NPs under concentration 5.980×10^{12} ml^{-1}; (b) 100 nm diameter NPs under concentration 3.835×10^{9} ml^{-1}; (c) 400 nm diameter NPs under concentration 1.850×10^{8} ml^{-1}.

figure, the results for 10 and 100 nm size gold NPs have been multiplied by suitable factors. The yellow line shows the results of scattered light 10 nm gold NPs and it is about 0.4 pW at Z distance 5.49 mm. The red line shows the results of scattered light 100 nm gold NPs and it is about 300 pW at a Z distance of 5.49 mm. The blue line shows the results of scattered light 400 nm gold NPs and it is about 34.7 nW at a Z distance of 5.49 mm. The black circle with an error bar shows the error region of the calculated values due to the concentration

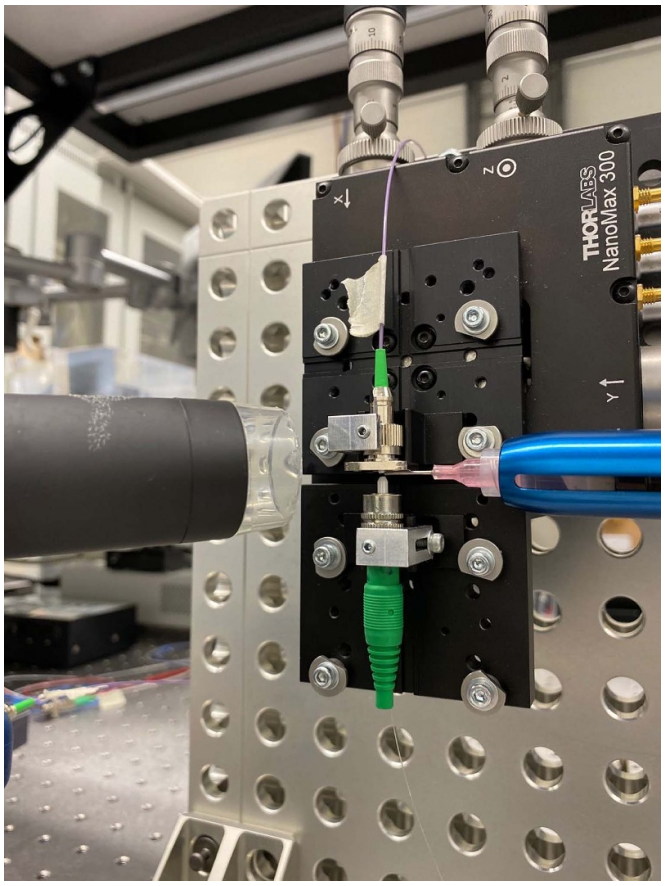

Figure 7. Photo of the designed setup. The upper optical fibre and the lower optical fibre are assembled in angle polished connectors (green) respectively clamped on the 3-axis stage with special designed clamps. The syringe in the volumetric dispenser used to drop liquid with a USB microscope to obtain the view for dropping liquid.

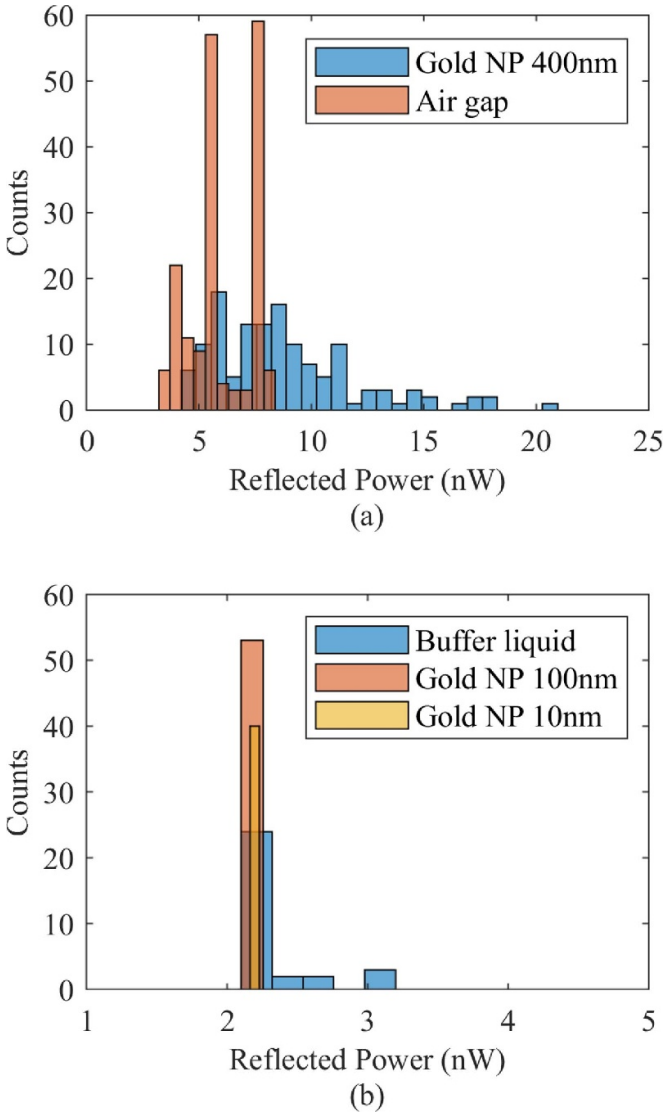

Figure 8. Experiment results of obtained reflected signals. (a) Comparison of air gap (without dropping liquid) and 400 nm gold NP suspension; (b) comparison of buffer liquid, 100 nm gold NP suspension and 10 nm gold NP suspension.

distribution of 400 nm gold NP suspension. The blue circle represents the mean value of the scattered light from 400 nm gold NP which has been subtracted from the other reflections by the data of obtained reflected power with buffer liquid and has also been modified by taking the light loss due to the optical circulator. The error bars of the blue circle show the position error range and the detected values range. The mean values of the 100 nm gold NPs and 10 nm gold NPs cases are almost 0 and are not shown in figure 9(a).

Figure 9(b) shows the reflected power within each axial resolution. The solid lines show the results of scattered light by NPs in water and the dotted lines shows the cases for RI matching liquid (RI is 1.4520). The values for different liquids are similar. For 10 nm gold NPs, the scattered light decreases along the Z direction from about -105 dB to about -130 dB. For 100 nm gold NPs, the scattered light decreases from about -75 dB to about -100 dB. For 400 nm gold NPs, the scattered light decreases from about -55 dB to about -85 dB.

4. Discussion

From the simulation results in figure 5, when the sizes of the gold NPs decrease from 400 nm to 10 nm, the accumulated scattered power at the same Z distance decreases dramatically. It shows that the larger size gold NPs scattered much more light than the smaller particles (especially for NPs smaller than 50 nm). The accumulated scattered power increases but the increase rate becomes slow because more scattered light is accumulated when the Z distance is larger and when the Z distance increases the light divergence in space will cause a lower power density to the incident on the NPs so that there is less scattered light by each NP and the coupling efficiency will decrease when the Z distance increases. It is also shown in figure 6 that most of the scattered light received by the upper optical fibre occurs at the region near the upper optical fibre end tip.

The experimental results in figure 8 show a larger dispersion for the case of the 400 nm gold NP suspension than is the cases for the 100 nm gold NP suspension and the 10 nm gold NP suspension. It implies a larger spatial distribution nonuniformty for larger size gold NPs.

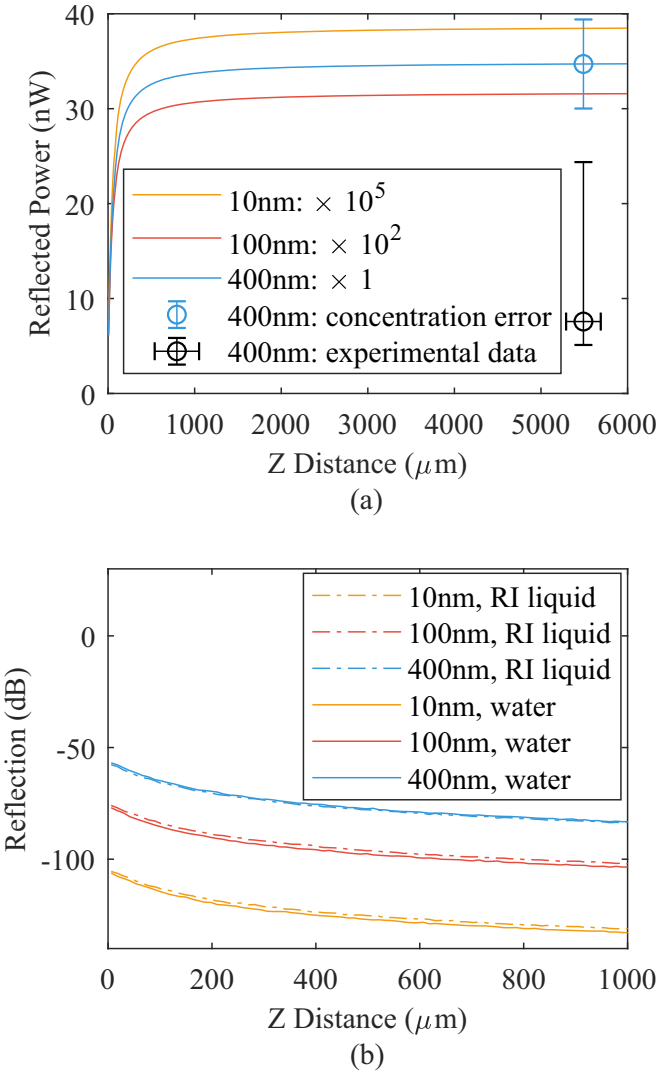

Figure 9. Estimated reflection values along the Z direction with resolution 12 μm compared with experimental results. The concentration of 10 nm diameter gold NPs is 5.980×10^{12} ml^{-1}; the concentration of 100 nm diameter gold NPs is 3.835×10^{9}ml^{-1}; the concentration of 400 nm diameter gold NPs is 1.850×10^{8}ml^{-1}. The incident power at the upper optical fibre is 3 mW. (a) The accumulated results along the Z direction for gold NPs in water; (b) the calculated results for gold NPs in water and RI matching liquid (RI = 1.4520) with resolution 12 μm.

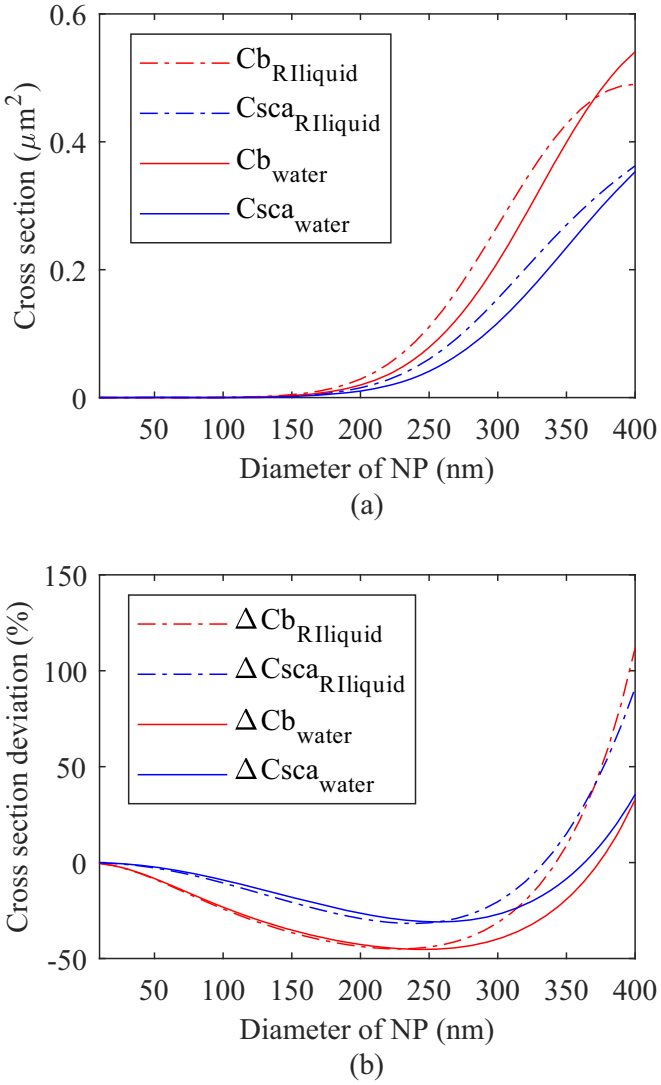

Figure 10. The comparison with Mie and Rayleigh theory in cross sections. (a) The backward scattering cross section (*Cb*) and the scattering cross section (*Csca*) with Mie theory for different sizes of NPs in RI liquid or in water; (b) the deviations between the cross sections calculated by Rayleigh and Mie theory. The diameters of NPs are from 10 to 400 nm.

The calculated accumulated reflected power in figure 9(a) shows that at a Z distance of 5.49 mm the accumulated reflected power from 10 nm gold NPs is about 0.4 pW. For 100 nm gold NPs, it is about 300 pW. Both of them cannot be detected by photodetector PM20C which has a detection limit of −65 dBm [33]. For the 400 nm gold NPs, it is about 34.71 nW. The blue circle with the error bar shows the predicted values from the model when the concentration error is considered. However, the experimental data shown by a black circle with error bars is below the expected value. The maximum experimental data is about 31.6% lower than the expected value. This loss is maybe caused by a lower concentration of gold NPs in the syringe because of the deposition of large size gold NPs and clusters of these gold NPs. In addition, it maybe also caused by the absorption by water which was neglected in the calculations. When absorption by water is considered ($\alpha = 2.6$ mm^{-1} [34]), the expected reflected value is 24.76 nW and it is slightly above the experimental data range (from 5.11 nW to 24.37 nW).

It can be seen from figure 9(b) that the scattered light distribution from 400 nm gold NPs is different from the scattered light from smaller size (10 nm and 100 nm) gold NPs. The scattered light by 400 nm in water is slightly higher than the scattered light by 400 nm in RI liquid. However, for 10 and 100 nm gold NPs, the scattered light in water is lower than the scattered light in RI liquid. It is caused by the change in distribution of the scattered light in all directions when the sizes of the NPs increase which can be seen from figure 10(a). Figure 10(a) shows the cross sections of different sizes of NPs

in water and in RI liquid with the 1550 nm central wavelength broadband light source. It can be seen from figure 10(a) that when the size of NPs increases to about 400 nm, the backscattering cross sections in water (Cb_{RIwater}) exceed the backscattering cross sections in RI liquid. This means more light is scattered in water than in RI liquid. It corresponds to the case of 400 nm in water and in RI liquid in figure 9(b). It also can be seen from figure 10(a) that, for the cases of gold NPs in the RI liquid, the backscattering cross sections (Cb_{RIliquid}) are larger than their cross sections ($Csca_{\mathrm{RIliquid}}$) shown in dash dot lines, which refers to the asymmetry for the forward light scattering and backward light scattering and that more scattered light is towards the backscattering direction for diameters of NPs below 400 nm. It is similar for the cases of NPs in water. The backscattering cross sections in water (Cb_{RIwater}) are larger than their cross sections ($Csca_{\mathrm{RIwater}}$) shown in solid lines.

For small size NPs, the Rayleigh scattering formula can be used for the calculation of the scattered light by NPs as an approximation. However, it will cause non-negligible deviations in our simulations even though the sizes of the gold NPs are relatively small (10–400 nm) compared with the incident light (around 1550 nm). Figure 10(b) shows the deviations by the deviations of cross sections (ΔC) with Rayleigh and with Mie theory. It can be seen from figure 10(b) that for the scattering cross sections ($\Delta Csca_{\mathrm{water}}$ and $\Delta Csca_{\mathrm{RI\ liquid}}$), Rayleigh scattering can be used for the calculation from 10(b). However, for the backscattering cross sections in water and in RI liquid ($\Delta Cb_{\mathrm{water}}$ and $\Delta Cb_{\mathrm{RI\ liquid}}$) even for small sizes of NPs (below 100 nm) there are non-negligible deviations. Therefore, Mie theory is used for the calculations in this paper.

For the cases of 10 nm gold NPs and 100 nm gold NPs as shown in figure 9(b), higher sensitivity detection methods need to be used. For example, a single photon detector or interferometer can be used. Generally, OCT has the advantage of a high sensitivity for detecting low signals. The sensitivities of some OCT systems can reach above 100 dB sensitivity [35–37]. This high sensitivity is enough for the detection for the signals of the 100 nm gold NPs in figure 9(b), but for the case of 10 nm gold NPs it is still a challenge. Therefore, the challenge of the detection of such weak intensity scattered light remains.

For the commonly used optical fibre single mode fibre SMF-28, the backscattering signal is as low as -100 dB mm^{-1} [10] (about -120 dB/12 μm). Compared with the simulation results shown in figure 9(b), even for the case of 10 nm gold NPs in figure 9(b) to doping optical fibre, the backscacttering signal will increase a lot (14 dB). Although the relationship between the increase of the signal and the strain sensing performance still needs to be investigated, from the experimental results from Loranger *et al* [11], a 20 dB signal increase causes an order-of-magnitude increase in strain resolution, which has potential for fibre optic sensing. For the cases of 100 nm gold NPs and 400 nm gold NPs, the backscattering signal will increase about 43 dB and about 61 dB respectively, which are much higher than the previously mentioned 20 dB. In addition, by changing the concentration of the NPs it may also be possible to achieve a control of the backscattering signals in the optical fibre that can be used for some critical areas of the materials for SHM.

5. Conclusions

A scattered light coupling model for the setup of dropping refractive index matching liquid containing NPs onto optical fibre interfaces is proposed. By simulation, the values of reflections along the Z direction for different sizes of gold NPs from 10 to 400 nm are obtained. Experiments with commercial gold NP suspensions were used to evaluate the model and the results are close to the calculated results but slightly lower, which may be caused by the deposition of NPs. The size parameter shows an important influence on the intensity of scattered light by NPs and the intensity of scattered light will increase dramatically when the size of NPs increase. For low concentration large size NPs (400 nm diameter gold NPs in experiments) the scattered signal can be detected while for low scattering from small particles (10 nm diameter) is still a challenge.

Acknowledgments

The authors gratefully acknowledge financial support from the China Scholarship Council (No. 201806020197).

ORCID iDs

Xiang Wang https://orcid.org/0000-0003-4889-4501
Roger M Groves https://orcid.org/0000-0001-9169-9256

References

[1] Froggatt M and Moore J 1998 *Appl. Opt.* **37** 1735–40
[2] Soller B, Gifford D, Wolfe M, Froggatt M, Yu M and Wysocki P 2006 Measurement of localized heating in fiber optic components with millimeter spatial resolution *2006 Optical Fiber Conf. and the National Fiber Optic Conf.* (IEEE)
[3] Song J, Li W, Lu P, Xu Y, Chen L and Bao X 2014 *IEEE Photonics J.* **6** 1–8
[4] Wang S, Lasn K, Elverum C W, Wan D and Echtermeyer A 2020 *Addit. Manuf.* **32** 101040
[5] Sante R D 2015 *Sensors* **15** 18666–713
[6] Bueno P M, Martinez M, Rans C and Benedictus R 2016 *Adv. Mater. Res.* **1135** 1–19
[7] Güemes A, Fernandez-Lopez A and Fernandez P 2014 Damage detection in composite structures from fibre optic distributed strain measurements *EWSHM—7th European Workshop on Structural Health Monitoring*
[8] Barrias A, Casas J and Villalba S 2016 *Sensors* **16** 748
[9] Güemes A, Fernández-López A and Soller B 2010 *Struct. Health Monit.* **9** 233–45
[10] Lu P, Mihailov S J, Coulas D, Ding H and Bao X 2019 *J. Lightwave Technol.* **37** 4697–702
[11] Loranger S, Gagné M, Lambin-Iezzi V and Kashyap R 2015 *Sci. Rep.* **5** 11177
[12] Parent F, Loranger S, Mandal K K, Iezzi V L, Lapointe J, Boisvert J S, Baiad M D, Kadoury S and Kashyap R 2017 *Biomed. Opt. Express* **8** 2210
[13] Yan A, Huang S, Li S, Chen R, Ohodnicki P, Buric M, Lee S, Li M J and Chen K P 2017 *Sci. Rep.* **7** 1–9
[14] Lu P, Mihailov S J, Coulas D, Ding H and Bao X 2018 Random fiber gratings fabricated using Fs-IR laser for distributed temperature sensor application *26th Int. Conf. Optical Fiber Sensors* (OSA)

[15] Blanc W and Dussardier B 2015 *J. Opt.* **45** 247–54
[16] Molardi C, Korganbayev S, Blanc W and Tosi D 2018 Characterization of a nanoparticles-doped optical fiber by the use of optical backscatter reflectometry *Advanced Sensor Systems and Applications VIII* vol 10821 (International Society for Optics and Photonics) p 1082121
[17] Beisenova A, Issatayeva A, Iordachita I, Blanc W, Molardi C and Tosi D 2019 *Opt. Express* **27** 22074
[18] Wang X, Benedictus R and Groves R M 2020 Light scattering and rheological effects in an optical fibre coupled nanoparticle suspension *Optical Sensing and Detection VI* vol 11354 (International Society for Optics and Photonics) p 113540V
[19] García J, Monzón-Hernández D, Manríquez J and Bustos E 2016 *Opt. Mater.* **51** 208–12
[20] Wu W T, Chen C H, Chiang C Y and Chau L K 2018 *Sensors* **18** 1759
[21] Kim H M, Jeong D H, Lee H Y, Park J H and Lee S K 2019 *Opt. Laser Technol.* **114** 171–78
[22] Zhang R, Pu S and Li X 2019 *Sensors* **19** 4345
[23] Quirantes A, Arroyo F and Quirantes-Ros J 2001 *J. Colloid Interface Sci.* **240** 78–82
[24] Bohren C F and Huffman D R 1998 *Absorption and Scattering of Light by Small Particles* (New York: Wiley)
[25] Bauer W F 1958 *J. Soc. Ind. Appl. Math.* **6** 438–51
[26] Herrador M A, Asuero A G and González A G 2005 *Chemometr. Intell. Lab. Syst.* **79** 115–22
[27] Johnson P B and Christy R W 1972 *Phys. Rev.* B **6** 4370–79
[28] Liu P 2014 *Optical Coherence Tomography for Material Characterization* PhD Thesis TU Delft
[29] www.thorlabs.com/thorproduct.cfm?partnumber=1550BHP
[30] https://cargille.com/wp-content/uploads/2018/06/Refractive-Index-Liquid-Series-A-n-1.4620-at-589.3-nm-and-25
[31] Matzler C 2002 *IAP Res. Rep.* **8** 1–17
[32] www.sigmaaldrich.com
[33] www.thorlabs.com/thorproduct.cfm?partnumber=PM20C#ad-image-0
[34] Curcio J A and Petty C C 1951 *JOSA* **41** 302–304
[35] Tanaka M, Hirano M, Murashima K, Obi H, Yamaguchi R and Hasegawa T 2015 *Opt. Express* **23** 6645–55
[36] Blatter C, Grajciar B, Huber R and Leitgeb R A 2011 Structural and functional imaging with extended focus dark-field OCT at 1300nm *Optical Coherence Tomography and Coherence Domain Optical Methods in Biomedicine XV* vol 7889 (International Society for Optics and Photonics) p 78891D
[37] Moayed A A, Hariri S, Choh V and Bizheva K 2011 *Opt. Lett.* **36** 4575–77